

A unique isolated dwarf spheroidal galaxy at $D=1.9$ Mpc

Dmitry Makarov^{1*}, Lidia Makarova¹, Margarita Sharina¹, Roman Uklein¹,

Anton Tikhonov², Puragra Guhathakurta³, Evan Kirby⁴ and Natalya Terekhova⁵

¹*Special Astrophysical Observatory, Nizhniy Arkhyz, Karachai-Cherkessia 369167, Russia*

²*Saint-Petersburg State University, Russia*

³*UCO/Lick Observatory, University of California-Santa Cruz, Santa Cruz, CA 95064, USA*

⁴*California Institute of Technology, 1200 E. California Blvd., MC 249-17, Pasadena, CA 91125, USA*

⁵*Sternberg Astronomical Institute, Moscow State University, Russia*

ABSTRACT

We present a photometric and spectroscopic study of the unique isolated nearby dSph galaxy KKR25. The galaxy was resolved into stars with HST/WFPC2 including old red giant branch and red clump. We have constructed a model of the resolved stellar populations and measured the star formation rate and metallicity as function of time. The main star formation activity period occurred about 12.6 to 13.7 Gyr ago. These stars are mostly metal-poor, with a mean metallicity $[Fe/H] \sim -1$ to -1.6 dex. About 60 per cent of the total stellar mass was formed during this event. There are indications of intermediate age star formation in KKR25 between 1 and 4 Gyr with no significant signs of metal enrichment for these stars. Long-slit spectroscopy was carried out using the Russian 6-m telescope of the integrated starlight and bright individual objects in the galaxy. We have discovered a planetary nebula (PN) in KKR25. This is the first known PN in a dwarf spheroidal galaxy outside the Local Group. We have measured its oxygen abundance $12 + \log(O/H) = 7.60 \pm 0.07$ dex and a radial velocity $V_h = -79$ km s^{-1} . We have analysed the stellar density distribution in the galaxy body. The galaxy has an exponential surface brightness profile with a central light depression. We discuss the evolutionary status of KKR25, which belongs to a rare class of very isolated dwarf galaxies with spheroidal morphology.

Key words: galaxies: individual: KKR 25 - galaxies: dwarf - galaxies: distances and redshifts - galaxies: stellar content

1 INTRODUCTION

The isolated dwarf spheroidal galaxy KKR 25 was discovered by Karachentseva et al. (1999) during the search of dwarf galaxies in the direction of the Local Void. Follow-up observations with the 100-m radio telescope at Effelsberg (Huchtmeier et al. 2000, 2003) have shown HI emission in the object with a radial velocity $V_h = -139.5$ km s^{-1} . Direct images of this low surface brightness galaxy were obtained with the 6-meter telescope of the Special astrophysical observatory (SAO) of the Russian Academy of Sciences (Karachentsev et al. 2001) and with the Hubble Space Telescope (*HST*). Its colour-magnitude diagram (CMD) shows a red giant branch population and a trace of blue stars. Karachentsev et al. (2001) classify the object as transition type galaxy (dIrr/dSph) at the distance of 1.86 Mpc.

On the other hand, the spectral survey of nearby dwarf LSB galaxies with the Russian 6-m telescope failed to detect

an optical velocity of KKR 25 (Makarov et al. 2003). Moreover, deep radio observations with the Giant Metrewave Radio Telescope (GMRT) (Begum & Chengalur 2005) did not show significant HI emission in the range $-256 < V_h < -45$ km s^{-1} at the level $M_{HI} = 0.8 \times 10^5 M_\odot$. Begum & Chengalur (2005) concluded that ‘the non-detection of HI in KKR 25 suggests that previous single-dish measurements were affected by confusion with the Galactic emission. Our stringent limits on the HI mass of KKR 25 indicate that it is a normal dSph galaxy’.

KKR 25 is one of the most isolated galaxies inside the sphere of 3 Mpc around us. It settles at the distance of 1.9 Mpc from the Milky Way and at 1.2 Mpc above the SuperGalactic plane in the front of the Local Void. KKR 25 is far away from the zero-velocity surface of $R_0 = 0.96 \pm 0.03$ Mpc (Karachentsev et al. 2009), which separates the Local Group from the cosmic expansion. The Local Group is the nearest massive structure to KKR 25. The second close massive group is the M 81 at the distance of 2.56 Mpc. There are no galaxies closer than 1 Mpc to KKR 25 (see Fig. 1). The

* E-mail: dim@sao.ru

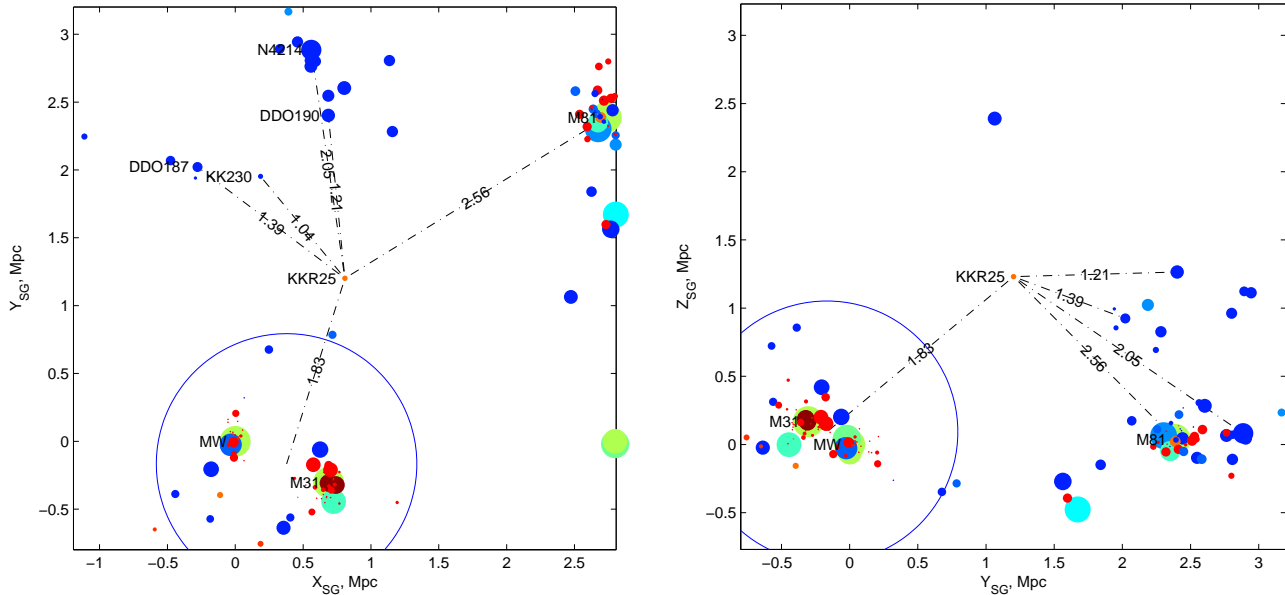


Figure 1. The map of galaxies in the SuperGalactic coordinates is centred on KKR 25. The left panel presents the projection of galaxies on the SuperGalactic plane, while the right panel shows the edge-on view on the ‘pancake’ of galaxies. The filled circle size is proportional to absolute magnitude of galaxies. Galaxies are coded by a colour from red for early types ($T = -5$) to blue for late types ($T = 10$), according to morphological type in de Vaucouleur’s numerical scale (de Vaucouleurs et al. 1991). The zero-velocity surface is shown by big blue circle around the Local Group. Distance to nearby structure is marked by dash-dotted lines with corresponding distance written on it. The brightest galaxies in the volume under consideration are Milky Way (WM), Andromeda galaxy (M31) and M81. They are signed on the figures. KK 230 is a closest galaxy to KKR 25. Three associations of dwarf galaxies (Tully et al. 2006) are shown on left panel. DDO 190 is the brightest member of 14+08 association. DDO 187 corresponds to ‘Dregs’ association and NGC 4214 to 14+07. The Local Void occupies the upper half of the right panel just above KKR 25.

nearest neighbour is the dwarf galaxy KK 230 ($M_B = -9.8$). The isolation of KKR 25 was pointed out by Karachentsev et al. (2001). Tully et al. (2006) note that KKR 25 is only isolated galaxy on the scale of 3 Mpc from us and ‘every object in this volume is associated with either a luminous group, an association of dwarfs, or the dregs evaporating association’. Two associations 14+08 (around DDO 190) and ‘Dregs’ (around DDO 187) stand on the distance of 1.2 and 1.4 Mpc from KKR 25, respectively.

In spite of its isolation KKR 25 has no gas and looks like a normal dwarf spheroidal system. This fact draws our attention, because we expect to find dSph galaxies in dense regions, like groups and clusters of galaxies. Obviously, that any kind of interaction with massive galaxy is not suitable to explain properties of KKR 25. This galaxy can play a crucial role in testing of different scenarios of dSph’s formation.

Karachentsev et al. (2001) have found a globular cluster candidate in the HST images of the galaxy. An apparent magnitude of the object $V_T = 20.59$ corresponds to $M_V = -5.79$, which is typical for Galactic globular clusters. In the framework of the $H\alpha$ survey of the Canes Venatici I cloud of galaxies with the Russian 6-m telescope Kaisin & Karachentsev (2008) also have found a faint $H\alpha$ knot on northern side of KKR 25. A measured flux of the knot is $\log F = -14.64 \text{ erg cm}^{-2} \text{ s}^{-1}$. These interesting objects were targeted for spectroscopic study with 6-m telescope in current study.

The main parameters of KKR 25 are presented in the

Table 1. Coordinates are taken from HyperLEDA¹ (Paturel et al. 2003). Apparent sizes were published by Karachentseva et al. (1999). The colour $(V - I)_T$ was measured by Karachentsev et al. (2001). The central surface brightness Σ_V was estimated from profiles published by Karachentsev et al. (2001). All other values, total magnitude V_T , axis ratio, scale length h , heliocentric velocity V_h and distance modulus $(m - M)_0$, are derived in the current work. The V_T , $(V - I)_T$ and Σ_V magnitudes are not corrected for Galactic extinction.

2 DIRECT IMAGES

2.1 Observations and photometry

KKR 25 was observed first with WFPC2 on 28 May 2001 as a part of the Hubble Space Telescope snapshot project (proposal 8601, PI: P. Seitzer). Two exposures were made with filters $F606W$ (broadband V) and $F814W$ (broadband I). The exposure time is 600 seconds in each filter. Later the galaxy was observed with WFPC2 on 23-25 March 2009 within the ANGST project (Dalcanton et al. 2009). Deep exposures in $F606W$ (4800s) and $F814W$ (9600s) were made. The image of KKR 25 is shown in Fig. 2. Stellar photometry procedures, artificial star experiments and star formation history (SFH) measurements were made for the both exposure sets. The results of the SFH measurements are in good

¹ <http://leda.univ-lyon1.fr/>

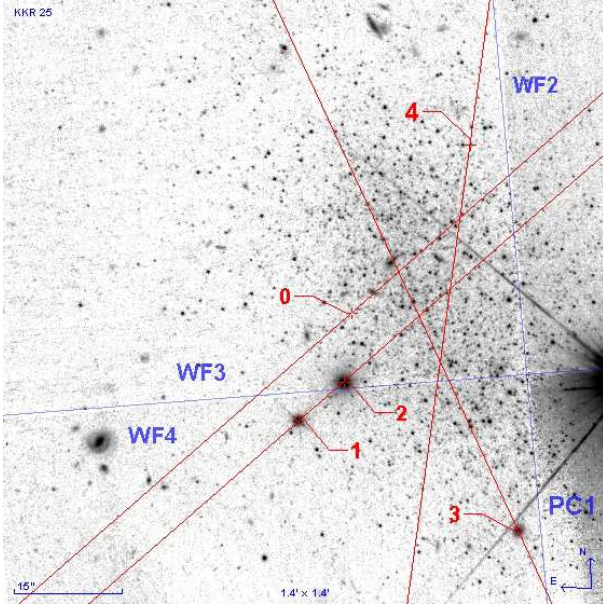


Figure 2. *HST* WFPC2 image of KKR 25 in *F814W* band. The bounds of planetary (PC1) and wide field cameras (WF2, WF3, WF4) are shown. Main part of KKR 25 is arranged in WF3 chip. A bright star fully saturates the PC1 camera. The objects for spectroscopic study are numbered. The long slit positions are overplotted. The integrated spectrum of the stellar light was obtained in the slit position ‘0’.

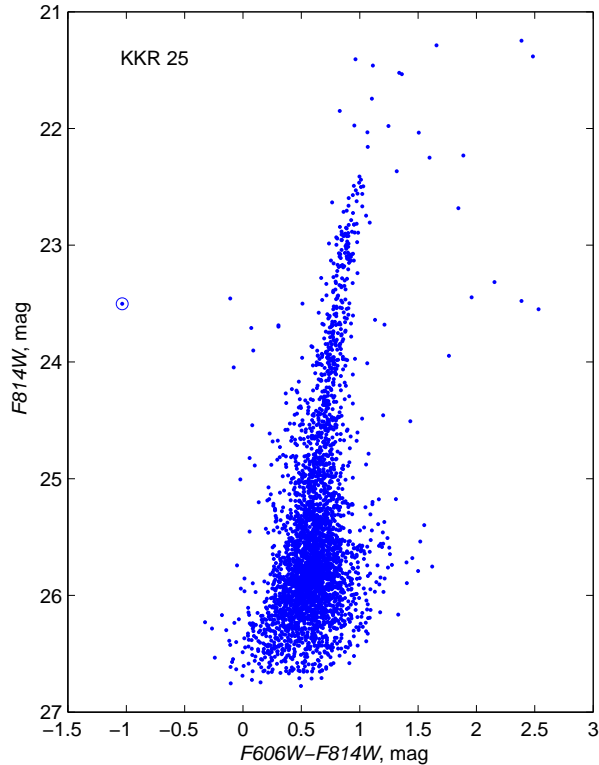


Figure 3. The colour-magnitude diagram based on *HST*/WFPC2 image of KKR 25. Extremely blue object 4 from our spectroscopic study is shown by open circle.

Table 1. Main parameters of KKR 25.

R.A. (J2000)	16 13 47.6	HyperLEDA
Dec (J2000)	+54 22 16	HyperLEDA
$E(B - V)$, mag	0.008	Schlegel et al. (1998)
Size, arcmin	1.1×0.65	Karachentseva et al. (1999)
h , arcsec	16.7 ± 1.1	this work
b/a	0.51 ± 0.03	this work
V_T , mag	15.52 ± 0.22	this work
$(V - I)_T$, mag	0.88	Karachentsev et al. (2001)
Σ_V , mag/arcsec ²	23.97 ± 0.03	Karachentsev et al. (2001)
V_h (stars), km s ⁻¹	-65 ± 15	this work
V_h (PN), km s ⁻¹	-79 ± 9	this work
$(m - M)_0$, mag	26.42 ± 0.07	this work
Distance, Mpc	1.93 ± 0.07	this work
V_{LG} , km s ⁻¹	128	this work
M_V , mag	-10.93	this work
L_V , $10^6 L_\odot$	2.0	this work
Σ_V , L_\odot pc ⁻²	9.6	this work

agreement. We have decided to consider only the deeper exposure data in this paper. All descriptions below are relate to the project 11986 (PI: J. Dalcanton) *HST*/WFPC2 images. The WFPC2 images were obtained from the STScI archive using the standard processing and calibration pipeline. A photometry of resolved stars in the galaxy was made with the *HSTPHOT* package (Dolphin 2000), following procedures and recipes indicated in the *HSTPHOT* Users Guide². The data quality images were used to mask bad pixels. Cosmic rays were masked using the *HSTPHOT crmask* utility. Only stars with photometry of good quality (signal-to-noise $S/N \geq 5$ in both filters, $|\chi| < 2.5$, $|\text{sharp}| < 0.3$ and type ≤ 2) were used in the analysis. Resulting colour-magnitude diagram (CMD) is presented in Fig. 3.

Artificial star tests were performed using the same reduction procedures to estimate photometric errors correctly. We have created a large library of artificial stars distributed in the same range of stellar magnitudes and colours as the original measured stars. Spatial distribution of the artificial stars also were resembling the original one so that the recovered photometry is adequately sampled. The photometric errors and completeness are represented in Fig. 4.

2.2 Reddening and background contamination

KKR 25 is situated at the rather high Galactic latitude and Galactic extinction is not large for this galaxy: $A_V = 0.028$ and $A_I = 0.016$ mag according to Schlegel et al. (1998). As can be seen from the colour-magnitude diagram of KKR 25, the field is not heavily contaminated by background stars. In order to estimate a number of foreground/background stars in the CMD, we have used *TRILEGAL* (Girardi et al. 2005) to simulate star counts in our Galaxy. *TRILEGAL* simulates CMDs in the WFPC2 instrumental system taking into account the components of thin and thick Galactic disks, the halo and the bulge of our Galaxy. The photometric errors, the saturation and the incompleteness were taken into account in the modelling. These models confirm a negligible contamination by foreground stars. An expected number of

² <http://purcell.as.arizona.edu/hstphot/hstphot.ps.gz>

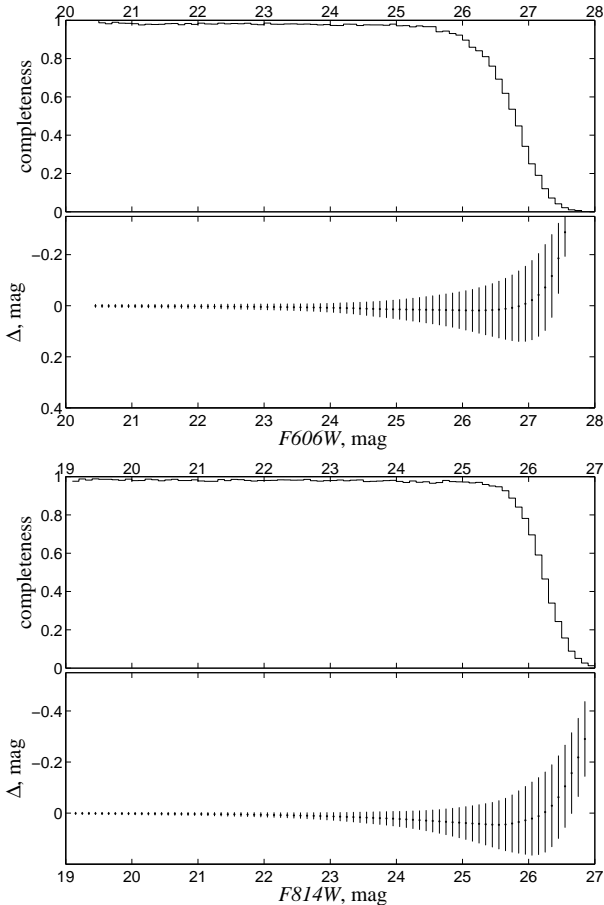


Figure 4. Photometric errors and completeness of KKR 25 in ANGST project. The photometry statistics were obtained using artificial star tests. The input, ‘true’ magnitude of artificial stars in $F606W$ and $F814W$ filters are shown on the abscissa. The completeness panel represents a fraction of detected artificial stars as function of input magnitude. The dispersion and bias of difference between ‘observed’ and ‘true’ magnitudes ($\Delta = m_{\text{obs}} - m_{\text{true}}$) are shown on bottom panels for both passbands.

foreground stars in the CMD is about 43 ± 6 up to the photometric limit $I = 27.0$ mag.

2.3 Distance determination

A photometric distance to KKR 25 was firstly estimated by Karachentsev et al. (2001) using tip of of the red giant branch (TRGB) distance indicator. They have obtained a true distance modulus $(m - M)_0 = 26.35 \pm 0.14$ mag and a respective distance $D = 1.86 \pm 0.12$ Mpc. TRGB distances for several galaxies in M 81 group were recently measured also by Dalcanton et al. (2009) within their ANGST project. However, the older dataset was used for their KKR 25 distance measurement in this paper. They determined a distance modulus of KKR 25 $(m - M)_0 = 26.43$.

The recent deep HST/WFPC2 observations and accurate HSTPHOT photometry allow us to estimate a TRGB distance with better uncertainties. TRGB method was also considerably improved recently. We have determined a photometric TRGB distance with our TRGBTOOL program, which uses a maximum-likelihood algorithm to determine

the magnitude of tip of the red giant branch from the stellar luminosity function (Makarov et al. 2006). The estimated value of TRGB is equal to $F814W = 22.41 \pm 0.07$ mag in the WFPC2 instrumental system. The uncertainty of the TRGB value estimation is dominated by poor statistics in the considered region of the colour-magnitude diagram. The calibration of the TRGB distance indicator was recently improved (Rizzi et al. 2007). Colour dependence of an absolute magnitude of TRGB and zero-point issues in HST/ACS and WFPC2 were addressed in the paper. Using this calibration, we have obtained the true distance modulus for KKR 25 $(m - M)_0 = 26.42 \pm 0.07$ mag and respective distance $D = 1.93 \pm 0.07$ Mpc. Both internal and calibration errors were taken into account in the error budget. The precision of the Galactic extinction value (16 per cent on the Schlegel’s maps) was also accounted. The new value is in good agreement with all the previous distance measurements.

2.4 Star formation history

The colour-magnitude diagram of KKR 25 (see Fig. 3) shows very tight and clean red giant branch, in the lower part of which, near the photometric limit ($F814W \sim 25.5$ – 26.5), we can see signs of a red clump. Judging from the CMD, we can expect low abundance and low age spread for the oldest stars in the galaxy. The extremely blue object in the CMD was classified by us as a planetary nebula belonging to KKR 25. The spectroscopic study of the PN is giving below.

First a star formation rate dependence from an age for KKR 25 was measured by Weisz et al. (2011) within their sample of 60 nearby galaxies. We determined detailed star formation history of KKR 25 from its CMD using our StarProbe package (Makarov & Makarova 2004). This program fits the observed photometric distribution of stars in the colour-magnitude diagram to a positive linear combination of synthetic diagrams of single stellar populations (SSPs, single age and single metallicity). The algorithm and the package are described in details in the paper of Makarov & Makarova (2004), and the package application to star formation history determination for some nearby galaxies are described in our work (Makarova et al. 2010). The observed data were binned into Hess diagram, giving number of stars in cells of the CMD. The size of the cells is 0.05 mag in luminosity and colour. The colour and magnitude limits of the constructed Hess diagram are $-0.3 < F606W - F814W < 2.5$, $21.0 < F814W < 26.8$. Synthetic Hess diagrams were constructed from theoretical stellar isochrones and initial mass function (IMF). We used the Padova2000 set of theoretical isochrones (Girardi et al. 2000), and a Salpeter (1955) IMF. We create a grid of the isochrones interpolated by age to fill gaps between the original isochrones. The original metallicity set was not altered. The distance was taken from the present paper (see above) and the Galactic extinction is from Schlegel et al. (1998). A binary fraction was assumed to be 30 per cents. The mass function of individual stars and the main component of a binary system is supposed to be the same. The mass distribution for second component was taken to be flat in the range 0.7 to 1.0 of the main component mass.

The synthetic diagrams were altered by the same incompleteness and crowding effects, and photometric system-

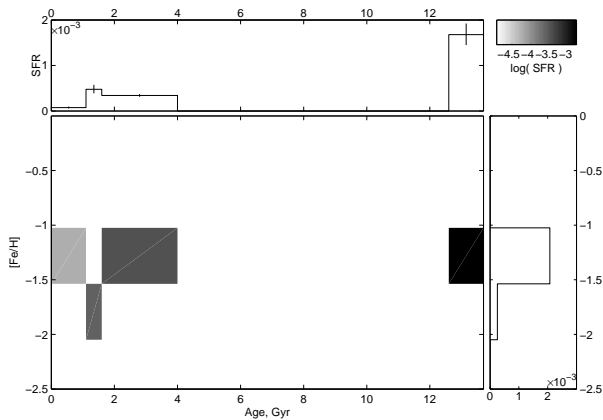


Figure 5. The star formation history of the dwarf galaxy KKR25. The top panel shows the star formation rate (SFR) (M_{\odot}/yr) against the age of the stellar populations. The bottom panel represents the metallicity of stellar content as function of age. The grayscale colour corresponds to the strength of SFR for given age and metallicity.

atics as those determined for the observations using artificial stars experiments. The synthetic diagrams covers all the range of ages (from 0 Myr to 13.7 Gyr) and metallicities (from $Z = 0.0001$ to $Z = 0.03$). The best fitting combination of synthetic CMDs is a maximum-likelihood solution taking into account the Poisson noise of star counts in the cells of Hess diagram. The resulting star formation history (SFH) is shown in the Fig. 5. The 1σ error of each SSP is derived from analysis of the likelihood function.

The star formation histories from our work and Weisz et al. (2011) are in general good agreement. The main difference is in duration of star formation episodes. Weisz et al. (2011) used 6 fixed periods of star formation for all 60 galaxies, while in our measurement we have sophisticated algorithm of star formation periods fitting. Firstly, we divided the galaxy lifetime into quite small steps (0.5 Gyr between 0 and 2 Gyr and 2 Gyr between 2 and 13.7 Gyr). In the resulting SFH we selected 5 episodes of star formation with constant SFR. A variation of bounds between these episodes of star formation allows to determine the best fitting of the models to the CMD.

According to our measurements, a main star formation event in KKR25 has occurred 12.6 – 13.7 Gyr ago with a mean star formation rate (SFR) $1.7 \pm 0.2 \times 10^{-3} M_{\odot} \text{ yr}^{-1}$. It is the total SFR over the whole galaxy. A metallicity range for the stars formed during this event is about $[\text{Fe}/\text{H}] = [-1.6 : -1]$ dex. This initial burst accounts for 62 per cents of the total mass of formed stars.

A quiescence period has appearing from about 4 to 12.6 Gyr ago. There are indications of intermediate age star formation in KKR25 between 1 and 4 Gyr with no significant signs of metal enrichment for these stars. A star formation rate is lower in this period and is equal $3.6 \times 10^{-4} M_{\odot} \text{ yr}^{-1}$. The measured star formation rate is very low for the recent 1 Gyr in this dwarf galaxy: $0.7 \pm 0.3 \times 10^{-4} M_{\odot} \text{ yr}^{-1}$. We found a total mass of the formed stars during KKR25 lifetime to be $3.0 \pm 0.3 \times 10^6 M_{\odot}$.

3 STRUCTURE OF THE GALAXY

Total and surface photometry of KKR25 are difficult tasks because of a bright foreground star at 20 arcsec from the centre of the galaxy. However, the HSTPHOT stellar photometry is reliable and affected by bright star much less. Moreover, this influence can be taken into account quantitatively.

We used the stellar photometry of the deep WFPC2 images to study a distribution of the stars in the galaxy. Our approach based on the maximum likelihood fit that was described by Martin et al. (2008). The likelihood function of stellar distribution in focal plane is defined as

$$\mathcal{L} = \prod_i^N l_i(p_1, p_2, \dots, p_k), \quad (1)$$

where $l_i(p_1, p_2, \dots, p_k)$ is probability to find a star i given by the set of parameters p_1, p_2, \dots, p_k with total number of stars N . This probability is determined by the surface density distribution of foreground and galactic stars, as well as the photometric completeness. Since KKR25 is located at the high Galactic latitude ($b = +44.4$) and the contamination of CMD by foreground stars is very insignificant we can neglect contribution of foreground objects. For the analysis we have selected only stars with $F814W < 26$, which corresponds to completeness level of about 80 per cent. We have tested the behaviour of completeness over the field of view. We did not find valuable variations in the body of the galaxy except for regions near brightest foreground stars. For instance, the bright foreground star affects the PC1 and partially WF2 cameras which is seen in Fig. 2. We excluded these regions from consideration. Distribution of stars in the areas under consideration is shown in the Fig. 6. The probability can be expressed in the form

$$l_i(p_1, p_2, \dots, p_k) = \Sigma(x_i, y_i | p_1, p_2, \dots, p_k) \quad (2)$$

$$N = \iint_D \Sigma(x, y | p_1, p_2, \dots, p_k) dx dy \quad (3)$$

where Σ is the model of surface density distribution with k parameters p_1, p_2, \dots, p_k and D is consideration domain.

We tested a set of models of surface density distribution: the exponential, exponential with central depression, King (1962), Plummer (1911) and Sersic (1968) profiles.

The WFPC2 coordinates of 1859 selected stars were corrected for the distortion and were transformed to the reference chip using *metric* procedure from STSDAS.HST_CALIB.WFPC package. For each model we derived a centre, position angle and axes ratio of the galaxy (4 parameters) as well as scale length parameters of the model (from 1 to 3 parameters). The central surface density is derived as normalisation coefficient to the total number of stars.

We used the Akaike Information Criterion $\text{AIC} = -2 \ln \mathcal{L} + 2k$ (Akaike 1974) and the Bayesian Information Criterion $\text{BIC} = -2 \ln \mathcal{L} + k \ln N$ (Schwarz 1978), where N is the sample size, i.e. the number of selected stars in our case. These criteria regulate the balance between the improvement of model by additional parameters and the number of parameters needed to achieve this improvement. One should prefer a model with a minimal value of the criterion. An absolute value of the criterion is not informative, while the difference between the AIC or BIC values for two fits provides an estimate of evidence for one model against another. The BIC difference $0 < \Delta_{\text{BIC}} < 2$ is not worth more

Table 2. A comparison of the different models of stellar population distribution of KKR25. Δ_{AIC} and Δ_{BIC} are computed respectively to the model with minimal value of the criterion.

Model	k	$\ln \mathcal{L}$	Δ_{AIC}	Δ_{BIC}
exp	5	-9963.4	43.6	38.1
exp 1	6	-9940.6	<u>0.0</u>	<u>0.0</u>
exp 2	7	-9940.3	1.5	7.0
Plummer	5	-9956.0	28.9	23.4
Sersic	6	-9949.2	17.2	17.2
King	6	-9946.4	11.7	11.7

Table 3. Parameters of the ‘exp 1’ model for different star selections. h is an exponential scale length, b/a is an axes ratio of the stellar distribution and R is the central depression radius.

	all	RGB	RC
	$F814W < 26$	$F814W < 25.5$	$25.5 < F814W < 26$
$h, ''$	$16.7^{+1.1}_{-1.0}$	$18.4^{+1.7}_{-1.4}$	$15.7^{+1.4}_{-1.3}$
h, pc	156^{+12}_{-11}	172^{+17}_{-14}	147^{+14}_{-13}
b/a	$0.51^{+0.03}_{-0.03}$	$0.46^{+0.04}_{-0.04}$	$0.55^{+0.05}_{-0.04}$
$R, ''$	$18.2^{+2.3}_{-3.1}$	$12.4^{+4.3}_{-6.4}$	$20.5^{+2.8}_{-2.8}$
R, pc	170^{+22}_{-30}	116^{+40}_{-60}	192^{+27}_{-27}

than a bare mention, $2 < \Delta_{\text{BIC}} < 6$ represents positive evidence, $6 < \Delta_{\text{BIC}} < 10$ means strong evidence and $\Delta_{\text{BIC}} > 10$ very strong evidence (Kass & Raftery 1995). There are similar guidelines for Δ_{AIC} values (Burnham & Anderson 2004). More details on a model selection can be found, for instance, in Liddle (2007).

A comparison of different models is presented in Table 2. The ‘exp 1’ and ‘exp 2’ code the models of exponential profile with central depression. These models differ from simple exponent within specific radius near the centre of the galaxy. The ‘exp 1’ corresponds to the model with a constant density in the centre, the ‘exp 2’ is an exponential decay in the central part of the galaxy. Taking into account only likelihood value, we can conclude that the pure exponential profile is the worst case of all. However, the simple modification of the exponential model with depression in the centre improves the fit significantly, and these models leave behind all other models under consideration. The AIC and BIC clearly select exponential profile with the constant surface density in the central region (exp 1) as the best fit model for the given distribution of the stars.

Stellar density profile of KKR25 is shown in Fig. 7. Structural parameters of the best model are summarized in the Table 3. The galaxy shows the exponential profile with axial ratio of 1:2 and flat distribution of the surface brightness near the centre. The angular size of the central depression roughly equals to the exponential scale length. We have estimated an integrated magnitude of the galaxy from the derived model parameters (see Table 3, ‘all’) and the central surface density $\Sigma_V = 23.97$ and $\Sigma_I = 23.09$ mag, which were taken from our previous photometry results (Karachentsev et al. 2001). We obtained the total magnitudes of KKR25 $V_T = 15.52 \pm 0.22$ and $I_T = 14.64 \pm 0.22$. The new V_T value is 0.4 mag brighter than $V_T = 15.9$ obtained by Karachentsev et al. (2001). The difference can be explained by difficulties

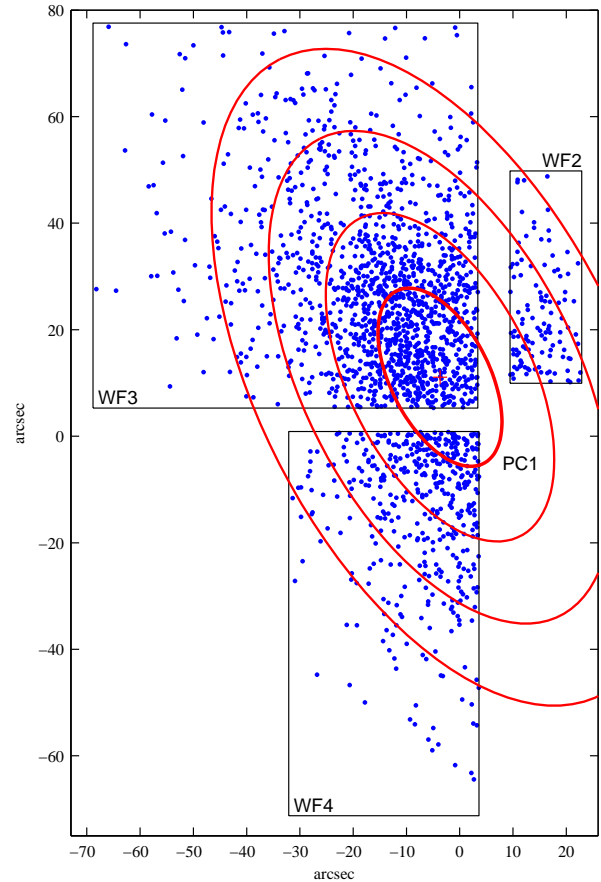


Figure 6. Distribution of the selected stars ($F814W < 26$) of KKR25 in the frame of WFPC2. The boxes represent the considered areas of the cameras WF2, WF3 and WF4. The PC1 camera affected by bright star and was not included in the analysis. The thick ellipse shows the size of central region of constant stellar density. The set of thin ellipses corresponds to 2, 3 and 4 times of the exponential scale length. The cross indicates the centre of the galaxy.

of photometry caused by nearby bright star and the small field of view where the galaxy occupies whole WFPC2 chip of WFPC2.

There is an indication on slightly different spatial distribution of red giant branch and red clump stars. These populations are indicated as RGB and RC in the Table 3, respectively. Judging from the scale length, the RC population is slightly more centrally concentrated than RGB stars. But the difference appears on level of two sigma.

4 SPECTROSCOPY

4.1 Observations and data reduction

We carried out several sets of long-slit observations of a globular cluster candidate, bright objects and $H\alpha$ source in KKR25. The spectroscopic data were obtained with the multi-mode focal reducer SCORPIO³ (Afanasiev & Moiseev 2005) in the prime focus of the Russian 6-m telescope.

³ <http://www.sao.ru/hq/lsvfo/devices/scorpio/scorpio.html>

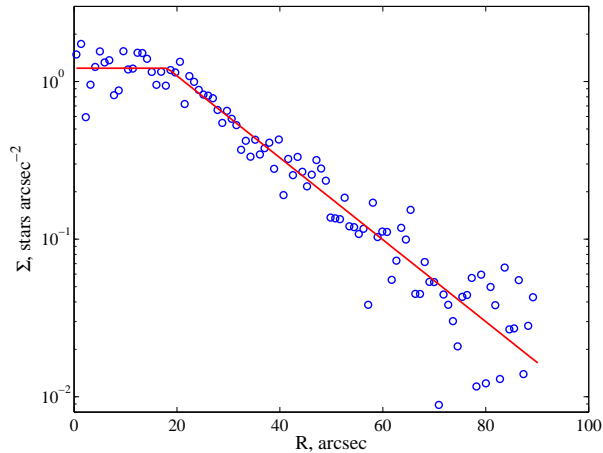


Figure 7. Surface density profile of the selected stars in KKR 25. The stellar density is measured in concentric elliptical annuli from the centre. The solid line represents the best fit model, the exponential profile with the depression in the central region. The parameters of the model were determined using maximum likelihood method.

Table 4. The journal of spectroscopic observations.

Object	Date	Exposure (s)	Seeing (″)
KKR 25 slit pos. 1–2	08/02/05	900 × 2	2.0
KKR 25 slit pos. 3	09/02/05	900 × 3	1.6
KKR 25 slit pos. 0	10/02/05	1200 × 3,900	2.5
KKR 25 slit pos. 4	30/05/09	1200 × 3,900	2.3
KKR 25	07/08/11	1200 × 3	1.5
Radial velocity standard stars			
BD +23 992	08/02/05	10	2.0
	09/02/05	10 × 2	2.0
	10/02/05	10 × 2	2.5
BD +23 680	08/02/05	10 × 2	2.0
BD +23 655	09/02/05	30 × 2	2.0
BD +23 751	10/02/05	10 × 2	2.5
BD +23 708	10/02/05	20	2.5
Spectroscopic standard stars			
SA 95–42	08/02/05	60	2.0
BD +75 325	09/02/05	30 × 2	2.0
	10/02/05	30 × 2	2.2
BD +33 2642	30/05/09	60	2.6
LDS 749 B	07/08/11	30 × 2	1.5

We used the grism VPHG550G (550 lines mm^{-1}) and $2\text{k} \times 2\text{k}$ CCD EEV42–40 detector. This combination together with the slit of $6' \times 1''$ provides a spectral resolution $\sim 10\text{\AA}$ in the range of $3500\text{--}7200\text{\AA}$. A typical dispersion was 2.1\AA per pixel. The frames were binned by 2 pixels along the slit direction, resulting in a spatial scale of 0.357 arcsec per pixel. For wavelength calibration we used He-Ne-Ar lamp.

The journal of observations is presented in Table 4. Orientations of the slit are shown on the direct WFPC2 image of the galaxy in Fig. 2.

The standard data reduction and analysis were performed using the European Southern Observatory Munich Image Data Analysis System⁴ (ESO-MIDAS) (Banse et al. 1983) and the Image Reduction and Analysis Facility (IRAF) software⁵. The dispersion solution determines an accuracy

⁴ <http://www.eso.org/sci/software/esomidas/>

⁵ <http://iraf.noao.edu/>

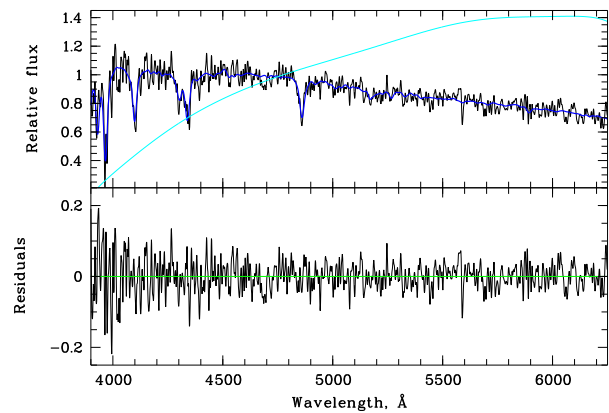


Figure 8. Top: Integrated spectrum of the stellar light of KKR 25 (black) in comparison with a composite model (dark-blue). The fitting is produced with the Vazdekis et al. (2010) SSP model and the Miles stellar library. The result of the division of the normalized model and object spectra is demonstrated in light-blue. Bottom: The difference between normalized observed and model spectra. The zero line is green.

of the wavelength calibration $\sim 0.14\text{\AA}$. The wavelength zero point can be shifted up to 2 pixels during the night. This effect was corrected using the night-sky lines in the dispersion-corrected spectra. An extraction of the spectra was made using the IRAF procedure *apsun*. After the wavelength calibration and sky subtraction, the spectra were corrected for atmospheric extinction and flux-calibrated using the observed spectrophotometric standard stars (Oke 1990). Finally, all one-dimensional spectra of each object were summed to increase the S/N ratio. We observed bright radial velocity standard stars (Barbier-Brossat & Figon 2000) at the end of each night to obtain heliocentric radial velocities of the program objects using the method of Tonry & Davis (1979), and to obtain the line-spread function (LSF) of the spectrograph.

4.2 Integrated stellar light of KKR 25

The spectra of integrated light of the KKR 25 were obtained during the observations on 10/02/2005 (Table 4). We combined these spectra with the data received in 2009 and 2011 years. The S/N per wavelength measured in the total integrated light spectrum at $\lambda \sim 5500\text{\AA}$ is 54, at $\lambda \sim 4000\text{\AA}$ is 15, and goes down at $\lambda \geq 5577\text{\AA}$ due to the bright emission sky lines. The resulting spectrum is demonstrated in black in Fig. 8 (top).

The STECKMAP program (Ocvirk et al. 2006a,b) with the PEGASE.HR model grids (Le Borgne et al. 2004) and the ULYSS⁶ program with the PEGASE.HR model grid and the Elodie (Prugniel & Soubiran 2001) and Miles (Sánchez-Blázquez et al. 2006) stellar libraries⁷, and Vazdekis (Vazdekis et al. 2010) SSP model with the Miles stellar library were employed to analyze stellar populations in KKR 25. We use Salpeter (1955) IMF in all these cases.

⁶ <http://ulyss.univ-lyon1.fr>

⁷ <http://ulyss.univ-lyon1.fr/models.html>

Table 5. List of spectroscopically observed objects. The columns are: (1) object number in Fig. 2; (2), (3) V-band magnitude and $V-I$ colour (HSTPHOT in the case of PN and aperture photometry in all other cases); (4) heliocentric radial velocity in km s^{-1} ; (5) classification.

N	R.A. (2000) Dec.	V	$V-I$	V_h	Note
1	161350.0+542201	21.6 ± 0.13	3.2 ± 0.10	-350 ± 52	star
2	161349.3+542206	20.5 ± 0.12	1.7 ± 0.10	100431 :	S0
3	161346.5+542145	21.3 ± 0.15	1.0 ± 0.25	224844 :	QSO
4	161347.2+542239	22.11 ± 0.11	-1.54 ± 0.14	-79 ± 9	PN

Comparison the fitting results for the three sets of models allows to claim that $\sim 70 - 100$ per cent of the light fraction in KKR 25 is as old as $2 - 14$ Gyr and has a low mean metallicity $[\text{Fe}/\text{H}] \sim -1.75 \pm 0.15$ dex. Unfortunately, because of low surface brightness of KKR 25 the night sky lines affect the resulting spectrum, especially in red part. Thus we can not reliably estimate a contribution and properties of the second stellar component with an age $1 - 2$ Gyr.

The one of three fittings is illustrated in Fig. 8, where a two-component model (Vazdekis et al. (2010) SSP model with the Miles stellar library) is shown in dark-blue. This model is completely composed of old metal-poor (age ~ 18 Gyr, $[\text{Fe}/\text{H}] = -1.68$ dex) population. The difference between the normalized object and model spectra (Fig. 8, bottom) is less equal 10 per cent. Broad absorption-line features are noticeable near 4227, 4455, ~ 4700 , 5036, ~ 5200 which were not fitted well by the models. They may be composed of TiO, Ca I, Mn I and Mg I lines. The relative intensity of such lines may indicate substantial α element enhancement, and the presence of dust in the interstellar medium blown out by previous generations of asymptotic-giant branch stars (Boyer 2008). The obtained $[\text{Fe}/\text{H}]$ is in good agreement with the stellar population CMD study presented in Sect. 2.4. We determined a radial velocity of the stellar component in KKR 25 is $V_h = -65 \pm 15 \text{ km s}^{-1}$.

4.3 Bright objects in the field of KKR 25

The diffuse globular cluster (GC) candidates (2, 3) and a very red star (1) were selected for spectroscopic survey using the snapshot *HST* images (see Fig. 2). Spectra of these objects were obtained with the 6-m telescope in 2005 (Table 4) in the framework of the project ‘Searches for GCs in nearby dwarf galaxies’ (PI: T.H. Puzia). The targets are indicated by numbers in Fig. 2. The candidate found by Karachentsev et al. (2001) has number 2 in our list. The results of the survey are summarised in the Table 5.

The spectra of GC candidates are shown in Fig. 9. We compared them with the templates of Kinney et al. (1996). The object selected by Karachentsev et al. (2001) appear to be a S0 galaxy with redshift $z \sim 0.335$. Another bright target is a quasar at $z \sim 0.75$.

The spectrum of the object 1 revealed the nature of this star as a M-type dwarf (see Fig. 10). Therefore it does not belong to KKR 25.

As a result of our survey we did not confirm the presence of globular clusters in KKR 25.

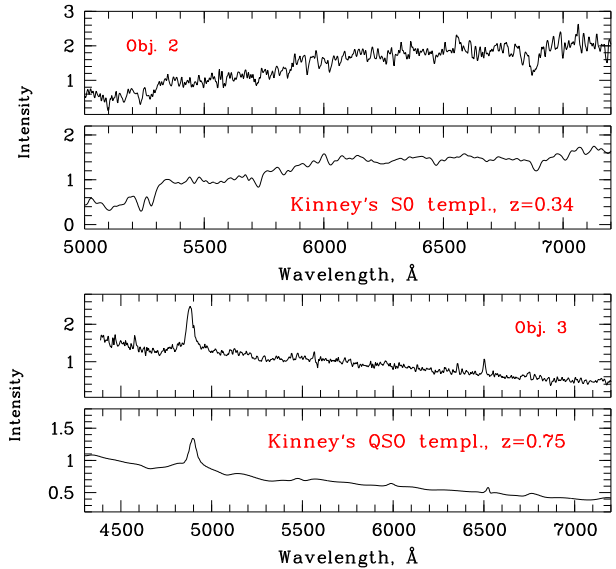


Figure 9. Spectra of background objects (2 and 3, Fig. 2) obtained at the 6-m telescope. Kinney et al. (1996) templates are shown for comparison.

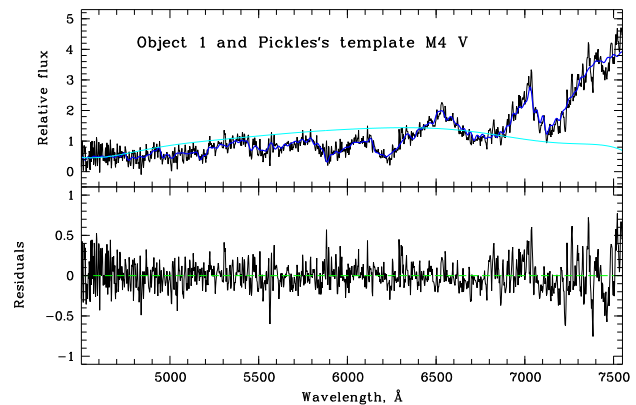


Figure 10. Spectrum of a bright red star near KKR 25. Top panel shows the observations (black) in comparison with normalized template (Pickles 1998) of M4V star (dark blue). The light-blue line demonstrates a multiplicative term applied to the original spectrum to bring it into the correspondence to the stellar template. The lower panel shows the fitting residuals.

4.4 $\text{H}\alpha$ object

A faint $\text{H}\alpha$ emission at the northern side of KKR 25 was discovered by Kaisin & Karachentsev (2008) in their $\text{H}\alpha$ survey of galaxies in the Canes Venatici I cloud. However, WFPC2 image does not show any extended object in the corresponding area of the galaxy. We identified $\text{H}\alpha$ object with unusual extremely blue star which is indicated with number 4 in the direct image (Fig. 2) and with a circle in the CMD (Fig. 3).

Taking into account that HSTPHOT perfectly fits this object with stellar profile ($\text{sharp} = -0.001$), and assuming that the object belongs to the galaxy, we can estimate an upper limit on linear size of $\text{H}\alpha$ source. Because the object profile is not wider than point spread function (PSF) we

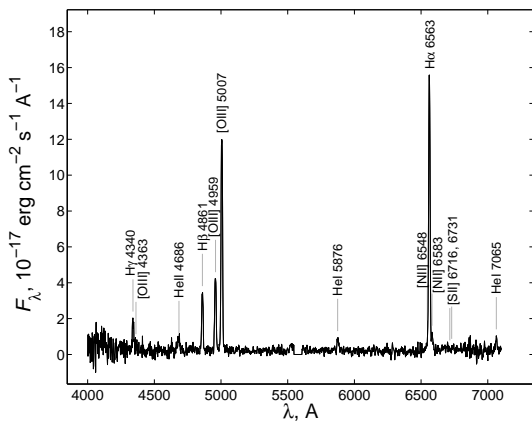


Figure 11. The spectrum of the $H\alpha$ object.

Table 6. Line intensities of the $H\alpha$ object.

Ion	λ , Å	$\frac{F(\lambda)}{F(H\beta)}$	$\frac{I(\lambda)}{I(H\beta)}$
H γ	4340.47	0.52 ± 0.08	0.66 ± 0.13
[O III]	4363.21	0.07 ± 0.05	0.08 ± 0.07
He II	4685.70	0.30 ± 0.07	0.32 ± 0.08
H β	4861.33	1.00 ± 0.08	1.00 ± 0.10
[O III]	4958.92	1.36 ± 0.10	1.30 ± 0.10
[O III]	5006.85	4.07 ± 0.26	3.82 ± 0.25
He I	5875.60	0.23 ± 0.05	0.16 ± 0.04
[N II]	6548.10	0.08 ± 0.04	0.04 ± 0.02
H α	6562.80	5.05 ± 0.30	2.80 ± 0.19
[N II]	6583.40	0.26 ± 0.06	0.14 ± 0.03
He I	7065.30	0.25 ± 0.05	0.12 ± 0.03

could assume that its angular size is smaller than the full width at half maxima (FWHM) for a stellar profile. Thus, $H\alpha$ source diameter should be less than 1.9 pc for WFPC2's FWHM $\sim 0.2''$ at the distance 1.93 Mpc. The median radius of old planetary nebulae (PN) is ~ 0.6 pc, while young PN typically have radii < 0.05 pc (Frew & Parker 2010). Although, H II regions have sizes from tens to hundreds parsecs (Oey et al. 2003), the ultra compact H II regions have diameters < 0.1 pc (Wood & Churchwell 1989), that comparable in size with PN.

Thus, intriguing question is the nature of the $H\alpha$ emission in KKR25. We carried out two sets of spectroscopic observations of the $H\alpha$ object with the 6-meter telescope on 30th May 2009 and 8th August 2011 (see Table 4). Each of 3 exposures of 1200 sec was obtained along the parallactic angle to minimize an influence of the atmospheric refraction. The resulting spectrum is shown in Fig. 11. Besides bright hydrogen and oxygen emissions we clearly see helium (He I 5876, 7065 and He II 4686) and nitrogen ([N II] 6548, 6583) lines. Table 6 presents measurements of the emission line intensities $F(\lambda)$ relative to $H\beta$, and the ratios corrected for Galactic and internal extinction ($I(\lambda)/I(H\beta)$).

Because the object under consideration is a point-like source, we can not use morphological properties for classification. Moreover, PN and H II spectra have the same emission lines. The difference is only in intensity ratios due to different temperature of central source. A central star in a PN is hotter than OB stars in H II regions. Kniazev et al. (2008a) proposed to use the following characteristic diagrams for the

separation of PN and H II regions (see formulas 1 and 3 from original publication):

$$\log \frac{[\text{O III}] 5007}{H\beta} \geq (0.61 / \log \frac{[\text{N II}] 6584}{H\alpha} - 0.47) + 1.19 \quad (4)$$

$$\log \frac{[\text{S II}] 6731, 6717}{H\alpha} \leq 0.63 \log \frac{[\text{N II}] 6584}{H\alpha} - 0.55 \quad (5)$$

These criteria allow to segregate 99 per cent of PNs from compact H II regions if an object satisfies to at least one of these inequalities. According to line intensity measurements (see Table 6) the $H\alpha$ object passes both criteria. The criterion (4) is satisfied at a level of 12 sigma. Because sulphur lines [S II] 6731, 6717 were not detected, we used 3σ upper limit for classification. $I([\text{S II}])/I(H\beta) < 0.06$ meets the criterion (5) at least on 4 sigma level. Thus, we can argue with high reliability that $H\alpha$ object is a planetary nebulae.

Using $H\alpha$ flux $\log F = -14.64 \text{ erg cm}^{-2} \text{ s}^{-1}$ from Kaisin & Karachentsev (2008) and $F([\text{O III}])/F(H\alpha)$ ratio from our measurements (Table 6), we can estimate visible $m_{5007} = -2.5 \log F - 13.74 = 23.09$ (Jacoby 1989), which corresponds to $M_{5007} = -3.35$ for a distance $(m - M)_0 = 26.42$ and $E(B - V) = 0.008$. Note, that the estimated absolute magnitude is close to bright cut-off of PN luminosity function.

We serendipitously discovered a planetary nebula in KKR25. PNs are not rare in giant galaxies. PN luminosity function is one of the popular methods for distance determination in the nearby Universe. There are number of irregular galaxies with known PNs as well as bright dwarf ellipticals NGC 185, NGC 205 near M 31. Up-to-date there are only 4 dwarf spheroidal system owning PN. It is NGC 147 (Gonçalves et al. 2007), a satellite of M 31, and Fornax (Kniazev et al. 2007), Sagittarius (Kniazev et al. 2008b) dwarf spheroidals and transitional type Phoenix (Saviane et al. 2009), are satellites of Milky Way. Most of these galaxies are significantly brighter than KKR25 and contain substantially bigger stellar mass. Only Sagittarius dSph and Phoenix are more less comparable with KKR25 by morphology and luminosity. We have found first PN in dSph galaxy outside the Local Group. An analysis of CMD on existence of extraordinary blue stars gives fast and easy method for selection of PN candidates in nearby galaxies.

We have estimated an oxygen abundance of PN to be $12 + \log(\text{O}/\text{H}) = 7.60 \pm 0.07$, using the semi-empirical method of Izotov & Thuan (2007). The line [O II] 3727 is invisible on our data. Thus, we estimated it as 2 sigma of noise in corresponding part of the spectrum. This contributions to total abundance of oxygen is negligible and variations of its intensity in range ± 1 sigma do not change the result.

The PN also allows us to measure velocity of the galaxy with high precision, which is really challenging for low surface brightness dwarf spheroidal galaxy without gas. We have estimated the heliocentric velocity of the $H\alpha$ object $V_h = -79 \pm 9 \text{ km s}^{-1}$ using weighted mean of redshifts of emission lines ($H\alpha$, $H\beta$ and [O III] 4959 and 5007) in each of 6 spectra obtained in 2009 and 2011 years with Russian 6-m telescope.

We have obtained spectra of $H\alpha$ spot in KKR25 with the DEMOS spectrograph on the Keck II 10-m telescope. The observations were carried out during 2 nights on February 22 and 23, 2009. We received 2×5 min spectra in the first and 3×5 min spectra in the second nights. The spectroscopic setup for the DEIMOS observations used the 1200

lines mm^{-1} grating with a central wavelength of 5800\AA . This provides a spectral coverage over a range of $4400 - 7100\text{\AA}$, with the dispersion about 0.33\AA per pixel. The observations took place against a very bright dawn sky. Nevertheless, each 5 min spectral exposure shows a bright emission line close to $\text{H}\alpha$ position. A weak $\text{N II } 6548$ line is also visible. There is only hint on $\text{N II } 6548$. We have estimated the heliocentric velocity $V_h = -54 \pm 12 \text{ km s}^{-1}$ using combined spectrum.

5 DISCUSSION

We gathered the properties of KKR 25, the Local Group spheroidals outside the virialized zones of Milky Way and M 31, and highly isolated dIrr KKH 98 in Table 7. The columns contain the galaxy identification; its morphological type; distance in Mpc from the Milky Way (MW), the Andromeda galaxy (M 31) and centroid of the Local Group (LG); tidal index (TI) and the main disturber as it defined by Karachentsev et al. (2004); absolute magnitude M_V ; central surface brightness Σ_V corrected for Galactic absorption; metallicity $[\text{Fe}/\text{H}]$; total mass M ; and mass-to-light ratio M/L_V . The original values were corrected for adopted distance if necessary. The tidal index characterizes in logarithmic scale the tidal influence from the most important nearby galaxy. The negative value corresponds to isolated object. KKR 25 is in 2.5 – 3 times brighter than Phoenix, Tucana and And XVIII, and in 1.5 times fainter than Cetus – the brightest isolated spheroidal. KKR 25 has the highest surface brightness of all spheroidal galaxies in our sample.

KKR 25 is very similar to remote dwarf spheroidal galaxies in the Local Group. Cetus, Tucana and And XVIII are the only dSphs which are not definitely satellites of the Milky Way or the Andromeda galaxy. All these galaxies are gas deficient. Any previous HI detections were disproved by direct observations of stellar kinematics of Cetus (Lewis et al. 2007) and Tucana (Fraternali et al. 2009), or by deep radio interferometric observations of KKR 25 (Begum & Chengalur 2005). Only in Phoenix, Gallart et al. (2001) concluded that a HI cloud was associated with the galaxy, but it has been lost after the last star formation episode. KKR 25 resides near the brightest end of luminosity function of dwarf spheroidals. It follows the same relation of surface brightness versus luminosity as satellites of Milky Way and M 31. We can expect that KKR 25 traces the same properties as isolated dSphs in the Local Group and has the similar mass and mass-to-light ratio.

In the Local Volume on the scale of a few Mpc we know only one galaxy comparable with KKR 25 in isolation. This highly isolated dwarf KKH 98 is a normal dIrr galaxy. $\text{H}\alpha$ emission indicates ongoing star formation rate $\log(\text{SFR}) = -3.5 M_\odot \text{ yr}^{-1}$ (Kaisin, private communication). The observations with GMRT in the framework of FIGGS project (Begum et al. 2008) detect $M_{\text{HI}} = 6.46 \times 10^6 M_\odot$ of neutral hydrogen which spreads over 1.4 kpc from the centre of the galaxy. A HI exceeds the optical size of KKH 98 in 3.45 times. A hydrogen mass-to-luminosity ratio $M_{\text{HI}}/L_V = 1$ is typical for dwarf galaxies of given luminosity. Using the data of Begum et al. (2008) ($W_{50} = 20.7 \text{ km s}^{-1}$, $i = 46^\circ$, $D_{\text{HI}} = 3.8'$), we estimated total indicative mass of KKH 98 $M = 6.6 \times 10^7 M_\odot$. The obtained mass is similar to the mass of isolated dwarf spheroidals. But KKH 98 shows very differ-

ent morphology, gas and star content. It seems mysterious why the galaxies of similar mass and resemble environment have so different star formation history.

During the search of field dwarf galaxies without signs of recent star formation in the luminosity range of $12 > M_r > 18$ mag and the stellar mass range of $10^7 < M_{\text{stellar}} < 10^9 M_\odot$ Geha et al. (2012) did not find such objects at distances above 1.5 Mpc from the central giant galaxy. Although KKR 25 lies below the lower limits both in the stellar mass and the luminosity, but quite close to them. KKR 25 is one of the most isolated galaxies in the vicinity of the Local Group. It does not contain a detectable amount of gas and can be reliably classified as dwarf spheroidal galaxy. Obviously, models of galaxy formation should take into account an existence of such objects. KKR 25 stays far away from any massive galaxy in the Local Volume to be affected by an interaction during its evolution. We can conclude that an evolution of KKR 25 was regulated by star formation in the galaxy itself rather than by its environment. The ‘primordial scenario’ proposed that dwarf spheroidals form before the reionization in small haloes $M < 2 \times 10^8 M_\odot$. A star formation in these haloes is regulated by cooling and feedback processes in the early Universe. Simulations of pre-reionization fossils explain main properties of dwarf spheroidals in the Local Group (Bovill & Ricotti 2009). It seems that KKR 25 is the best candidate of such a ‘fossil’ galaxy (Ricotti & Gnedin 2005).

Tikhonov & Klypin (2009) pointed out that the standard cosmological Λ CDM model predicts a factor of 10 more dwarf haloes in the field than the number of observed dwarf galaxies. Thus the theory meet the same problem as overabundance of dwarf dark matter haloes in the Local Group, so-called ‘missed satellites’ problem. Tikhonov & Klypin (2009) suggested several solutions. One of it implies significant incompleteness of the observational sample of galaxies. The model predicts 10 times more dwarf galaxies down to limiting magnitude $M_B = -12$ than listed in the Karachentsev et al. (2004) sample. Tikhonov & Klypin (2009) proposed that the dwarf spheroidal galaxies are good candidates for this role. Indeed, the sample of dIrrs seems to be complete down to the limit of $M_B = -12$ (Karachentsev et al. 2004). They hold significant amount of HI gas. An ongoing star formation increases surface brightness and total luminosity of a galaxy. Therefore, dIrrs are relatively easy to detect. At the same time, dSphs are invisible in blind HI surveys, they have very low surface brightness, which makes them extremely difficult to find. KKR 25 satisfies all these conditions as a first member of population of ‘missed’ galaxies. It is an isolated, gas deficient, low surface brightness, dwarf spheroidal galaxy. Taking into account only isolated spheroidal galaxies in the Local Group ($N \sim 2 - 4$), we can roughly estimate a total number of similar systems inside the Local Volume up to 8 Mpc. We could expect to find $N_t \sim 8^3 \times (2-4) \sim 1000-2000$ objects within the luminosity range $-9.5 > M_V > -11.5$. This number resembles the 1000 ‘missed’ dwarf spheroidals mentioned by Tikhonov & Klypin (2009). But it is necessary to point out that KKR 25 is one of the most luminous of known isolated dSphs. It has $M_B \approx -10$ and lies well above the photometric limit of $M_B < -12$. We could expect that other dSph galaxies will be even fainter. Therefore, it seems unlikely that galaxies similar to KKR 25 could solve the problem of ‘missed’ dwarfs.

Table 7. Properties of nearby isolated galaxies.

Galaxy ¹	Type ²	MW	M31	LG ³	TI ⁴	MD ⁵	M_V ⁶	Σ_V ⁷	[Fe/H] ⁸	M ⁹	M/L_V ¹⁰
		Mpc					mag	mag		$10^8 M_\odot$	M_\odot/L_\odot
KKR 25	dSph	1.93 ^a	1.87	1.86	-1.0	M31	-10.93 ^a	23.94 ^a			
Phoenix	Tr	0.42 ^b	0.86	0.58	0.7	MW	-9.95 ^c	24.3 ^l	-1.87 ± 0.06^b	0.31 ^c	37
Cetus	dSph	0.78 ^d	0.69	0.62	0.3	M31	-11.34 ^e	25.0 ^e	-1.9 ^f	1.1 ± 0.1^f	37
Tucana	dSph	0.88 ^d	1.34	1.09	-0.2	MW	-9.78 ^g	24.95 ^g	-1.7 ± 0.2^f	0.43 ± 0.15^f	62
And XVIII	dSph	1.36 ^h	0.61	0.94	0.4	M31	-9.7 ^h	$\leq 25.6^h$	-1.8 ± 0.1^f	0.27 ± 0.15^m	41
KKH 98	Irr	2.49 ⁱ	1.74	2.08	-0.9	M31	-12.23 ^j	22.6 ^j	-1.94 ^j	0.66 ^a	10

REFERENCES – ^a this work; ^b Hidalgo et al. (2009); ^c Mateo (1998); ^d Karachentsev et al. (2004); ^e McConnachie & Irwin (2006); ^f Kalirai et al. (2010); ^g Saviane et al. (1996); ^h McConnachie et al. (2008); ⁱ Melbourne et al. (2010) ^j Sharina et al. (2008); ^k Begum et al. (2008); ^l $\Sigma_B = 24.9$ (Lauberts & Valentijn 1989) has been transformed to V-band using $(B - V)_e = 0.61$ (Prugniel & Heraudeau 1998); ^m $M_{1/2} = 2.7 \times 10^7 M_\odot$ (Tollerud et al. 2011) is the mass at the half-light radius of the And XVIII.

¹ name of the galaxy;

² morphological type;

³ distance from the Milky Way (MW), the Andromeda galaxy (M31) and the centroid of the Local Group (LG) to the galaxy in Mpc;

⁴ tidal index;

⁵ main disturber;

⁶ V-band absolute magnitude of the galaxy;

⁷ V-band central surface brightness of the galaxy corrected for Galaxy absorption;

⁸ metallicity [Fe/H] of the galaxy;

⁹ total mass of the galaxy;

¹⁰ V-band total mass-to-luminosity ratio.

Anyway, the hunting for dwarf spheroidals in the field is an important task. An existence of dSph population in voids is the crucial test on models of formation and evolution of dwarf galaxies.

6 CONCLUSIONS

We present a photometric and spectroscopic study of the unique isolated nearby dSph galaxy KKR 25. Let us briefly summarize the results of our study. We have estimated the distance modulus of KKR 25 $(m - M)_0 = 26.42 \pm 0.07$ mag using the TRGB method. It corresponds to a distance $D = 1.93 \pm 0.07$ Mpc. The new value is in good agreement with all previous distance measurements.

We have derived a quantitative star formation history of the isolated dwarf spheroidal galaxy KKR 25. The star formation history was reconstructed using *HST*/WFPC2 images of the galaxy and a resolved stellar population modelling. According to our measurements, 62 per cent of the total stellar mass were formed during the initial burst of star formation occurred about 12.6 – 13.7 Gyr ago. There are indications of intermediate age star formation in KKR 25 between 1 and 4 Gyr with no significant signs of metal enrichment for these stars.

A distribution of the stars in the galaxy is well described by an exponential profile with central depression. The exponential scale length is $h = 156^{+12}_{-11}$ pc. The profile extends up to 5 scale lengths. The size of the depression $R = 170^{+22}_{-30}$ is about the exponential scale length.

We did not confirm the presence of globular clusters in KKR 25. In the fact, the previously selected candidates are background objects, S0 galaxy at $z = 0.34$ and QSO at $z = 0.75$.

The spectroscopy of H α object in KKR 25 revealed

that it is a planetary nebula with oxygen abundance $12 + \log(\text{O}/\text{H}) = 7.60 \pm 0.07$. We have serendipitously found the first PN in the dwarf spheroidal galaxy outside the Local Group. The search of extraordinary blue stars on CMD of stellar population gives the perspective method for selection of PN candidates in distant galaxies.

We have derived heliocentric velocity of KKR 25 using PN emission lines $V_h = -79 \pm 9$ and using integrated light of the galaxy $V_h = -65 \pm 15$.

Our study shows, that KKR 25 belongs to the population of highly isolated dwarf spheroidal galaxies, now rarely detected, but extremely important for our understanding of galaxy evolution theory.

The ‘primordial scenario’ of galaxy formation is preferable against tidal stripping mechanism to explain the isolation of KKR 25 and its morphology. Existence of big number of dwarf spheroidals in the field could explain the overabundance problem in modern simulations. The search for the dwarf spheroidal in voids is a crucial test for models of formation and evolution of dwarf galaxies.

ACKNOWLEDGEMENTS

We are thankful to Dr. S. Pustilnik for very useful discussions of our work. L.M. and D.M. are thankful to Else Starckenburg and Tjitske Starckenburg for very interesting and valuable discussion. We acknowledge the usage of the HyperLEDA database (<http://leda.univ-lyon1.fr>). STSDAS is a product of the Space Telescope Science Institute, which is operated by AURA for NASA. The work was supported by the Russian Foundation for Basic Research (RFBR) grant 11-02-00639, Russian-Ukrainian RFBR grant 11-02-90449, and the program no. 17 ‘Active

processes in galactic and extragalactic objects' of the Department of Physical Sciences of the Russian Academy of Sciences. We acknowledge the support of the Ministry of Education and Science of the Russian Federation, the contract 14.740.11.0901.

REFERENCES

- Afanasiev V. L., Moiseev A. V., 2005, *Astronomy Letters*, 31, 194
- Akaike H., 1974, *IEEE Transactions on Automatic Control*, 19, 716
- Banse K., Crane P., Grosbol P., Middleburg F., Ounnas C., Ponz D., Waldthausen H., 1983, *The Messenger*, 31, 26
- Barbier-Brossat M., Figon P., 2000, *A&AS*, 142, 217
- Begum A., Chengalur J. N., 2005, *MNRAS*, 362, 609
- Begum A., Chengalur J. N., Karachentsev I. D., Sharina M. E., Kaisin S. S., 2008, *MNRAS*, 386, 1667
- Bovill M. S., Ricotti M., 2009, *ApJ*, 693, 1859
- Boyer M. L., 2008, PhD thesis, University of Minnesota
- Burnham K. P., Anderson D. R., 2004, *Sociological Methods & Research*, 33, 261
- Dalcanton J. J., Williams B. F., Seth A. C., Dolphin A., Holtzman J., Rosema K., Skillman E. D., Cole A., Girardi L., Gogarten S. M., Karachentsev I. D., Olsen K., Weisz D., Christensen C., Freeman K., Gilbert K., Gallart C., Harris J., Hodge P., de Jong R. S., Karachentseva V., Mateo M., Stetson P. B., Tavares M., Zaritsky D., Governato F., Quinn T., 2009, *ApJS*, 183, 67
- de Vaucouleurs G., de Vaucouleurs A., Corwin Jr. H. G., Buta R. J., Paturel G., Fouqué P., 1991, *Third Reference Catalogue of Bright Galaxies. Volume I: Explanations and references. Volume II: Data for galaxies between 0^h and 12^h. Volume III: Data for galaxies between 12^h and 24^h.*
- Dolphin A. E., 2000, *PASP*, 112, 1383
- Fraternali F., Tolstoy E., Irwin M. J., Cole A. A., 2009, *A&A*, 499, 121
- Frew D. J., Parker Q. A., 2010, *PASA*, 27, 129
- Gallart C., Martínez-Delgado D., Gómez-Flechoso M. A., Mateo M., 2001, *AJ*, 121, 2572
- Geha M., Blanton M., Yan R., Tinker J., 2012, *ArXiv e-prints*
- Girardi L., Bressan A., Bertelli G., Chiosi C., 2000, *A&AS*, 141, 371
- Girardi L., Groenewegen M. A. T., Hatziminaoglou E., da Costa L., 2005, *A&A*, 436, 895
- Gonçalves D. R., Magrini L., Leisy P., Corradi R. L. M., 2007, *MNRAS*, 375, 715
- Hidalgo S. L., Aparicio A., Martínez-Delgado D., Gallart C., 2009, *ApJ*, 705, 704
- Huchtmeier W. K., Karachentsev I. D., Karachentseva V. E., 2000, *A&AS*, 147, 187
- , 2003, *A&A*, 401, 483
- Izotov Y. I., Thuan T. X., 2007, *ApJ*, 665, 1115
- Jacoby G. H., 1989, *ApJ*, 339, 39
- Kaisin S. S., Karachentsev I. D., 2008, *A&A*, 479, 603
- Kalirai J. S., Beaton R. L., Geha M. C., Gilbert K. M., Guhathakurta P., Kirby E. N., Majewski S. R., Ostheimer J. C., Patterson R. J., Wolf J., 2010, *ApJ*, 711, 671
- Karachentsev I. D., Karachentseva V. E., Huchtmeier W. K., Makarov D. I., 2004, *AJ*, 127, 2031
- Karachentsev I. D., Kashibadze O. G., Makarov D. I., Tully R. B., 2009, *MNRAS*, 393, 1265
- Karachentsev I. D., Sharina M. E., Dolphin A. E., Geisler D., Grebel E. K., Guhathakurta P., Hodge P. W., Karachentseva V. E., Sarajedini A., Seitzer P., 2001, *A&A*, 379, 407
- Karachentseva V. E., Karachentsev I. D., Richter G. M., 1999, *A&AS*, 135, 221
- Kass R. E., Raftery A. E., 1995, *Journal of the American Statistical Association*, 90, 773
- King I., 1962, *AJ*, 67, 471
- Kinney A. L., Calzetti D., Bohlin R. C., McQuade K., Storchi-Bergmann T., Schmitt H. R., 1996, *ApJ*, 467, 38
- Kniazev A. Y., Grebel E. K., Pustilnik S. A., Pramskij A. G., 2007, *A&A*, 468, 121
- Kniazev A. Y., Pustilnik S. A., Zucker D. B., 2008a, *MNRAS*, 384, 1045
- Kniazev A. Y., Zijlstra A. A., Grebel E. K., Pilyugin L. S., Pustilnik S., Väisänen P., Buckley D., Hashimoto Y., Loaring N., Romero E., Still M., Burgh E. B., Nordsieck K., 2008b, *MNRAS*, 388, 1667
- Lauberts A., Valentijn E. A., 1989, *The surface photometry catalogue of the ESO-Uppsala galaxies*, Lauberts, A. & Valentijn, E. A., ed.
- Le Borgne D., Rocca-Volmerange B., Prugniel P., Lançon A., Fioc M., Soubiran C., 2004, *A&A*, 425, 881
- Lewis G. F., Ibata R. A., Chapman S. C., McConnachie A., Irwin M. J., Tolstoy E., Tanvir N. R., 2007, *MNRAS*, 375, 1364
- Liddle A. R., 2007, *MNRAS*, 377, L74
- Makarov D., Makarova L., Rizzi L., Tully R. B., Dolphin A. E., Sakai S., Shaya E. J., 2006, *AJ*, 132, 2729
- Makarov D. I., Karachentsev I. D., Burenkov A. N., 2003, *A&A*, 405, 951
- Makarov D. I., Makarova L. N., 2004, *Astrophysics*, 47, 229
- Makarova L., Koleva M., Makarov D., Prugniel P., 2010, *MNRAS*, 406, 1152
- Martin N. F., de Jong J. T. A., Rix H., 2008, *ApJ*, 684, 1075
- Mateo M. L., 1998, *ARA&A*, 36, 435
- McConnachie A. W., Huxor A., Martin N. F., Irwin M. J., Chapman S. C., Fahlman G., Ferguson A. M. N., Ibata R. A., Lewis G. F., Richer H., Tanvir N. R., 2008, *ApJ*, 688, 1009
- McConnachie A. W., Irwin M. J., 2006, *MNRAS*, 365, 1263
- Melbourne J., Williams B., Dalcanton J., Ammons S. M., Max C., Koo D. C., Girardi L., Dolphin A., 2010, *ApJ*, 712, 469
- Ocvirk P., Pichon C., Lançon A., Thiébaud E., 2006a, *MNRAS*, 365, 74
- , 2006b, *MNRAS*, 365, 46
- Oey M. S., Parker J. S., Mikles V. J., Zhang X., 2003, *AJ*, 126, 2317
- Oke J. B., 1990, *AJ*, 99, 1621
- Paturel G., Petit C., Prugniel P., Theureau G., Rousseau J., Brouty M., Dubois P., Cambrésy L., 2003, *A&A*, 412, 45
- Pickles A. J., 1998, *PASP*, 110, 863
- Plummer H. C., 1911, *MNRAS*, 71, 460
- Prugniel P., Heraudeau P., 1998, *A&AS*, 128, 299
- Prugniel P., Soubiran C., 2001, *A&A*, 369, 1048
- Ricotti M., Gnedin N. Y., 2005, *ApJ*, 629, 259

- Rizzi L., Tully R. B., Makarov D., Makarova L., Dolphin A. E., Sakai S., Shaya E. J., 2007, *ApJ*, 661, 815
- Salpeter E. E., 1955, *ApJ*, 121, 161
- Sánchez-Blázquez P., Peletier R. F., Jiménez-Vicente J., Cardiel N., Cenarro A. J., Falcón-Barroso J., Gorgas J., Selam S., Vazdekis A., 2006, *MNRAS*, 371, 703
- Saviane I., Exter K., Tsamis Y., Gallart C., Péquignot D., 2009, *A&A*, 494, 515
- Saviane I., Held E. V., Piotto G., 1996, *A&A*, 315, 40
- Schlegel D. J., Finkbeiner D. P., Davis M., 1998, *ApJ*, 500, 525
- Schwarz G., 1978, *Annals of Statistics*, 6, 461
- Sersic J. L., 1968, *Atlas de galaxias australes*, Sersic, J. L., ed.
- Sharina M. E., Karachentsev I. D., Dolphin A. E., Karachentseva V. E., Tully R. B., Karataeva G. M., Makarov D. I., Makarova L. N., Sakai S., Shaya E. J., Nikolaev E. Y., Kuznetsov A. N., 2008, *MNRAS*, 384, 1544
- Tikhonov A. V., Klypin A., 2009, *MNRAS*, 395, 1915
- Tollerud E. J., Beaton R. L., Geha M. C., Bullock J. S., Guhathakurta P., Kalirai J. S., Majewski S. R., Kirby E. N., Gilbert K. M., Yniguez B., Patterson R. J., Osthheimer J. C., Choudhury A., 2011, *ArXiv e-prints*
- Tonry J., Davis M., 1979, *AJ*, 84, 1511
- Tully R. B., Rizzi L., Dolphin A. E., Karachentsev I. D., Karachentseva V. E., Makarov D. I., Makarova L., Sakai S., Shaya E. J., 2006, *AJ*, 132, 729
- Vazdekis A., Sánchez-Blázquez P., Falcón-Barroso J., Cenarro A. J., Beasley M. A., Cardiel N., Gorgas J., Peletier R. F., 2010, *MNRAS*, 404, 1639
- Weisz D. R., Dalcanton J. J., Williams B. F., Gilbert K. M., Skillman E. D., Seth A. C., Dolphin A. E., McQuinn K. B. W., Gogarten S. M., Holtzman J., Rosema K., Cole A., Karachentsev I. D., Zaritsky D., 2011, *ApJ*, 739, 5
- Wood D. O. S., Churchwell E., 1989, *ApJS*, 69, 831

This paper has been typeset from a $\text{\TeX}/\text{\LaTeX}$ file prepared by the author.